

SYNTHETIC BIOLOGY

Artificial kinetochore beads establish a biorientation-like state in the spindle

Kohei Asai^{1,2}, Yuanzhuo Zhou^{1,2}, Osamu Takenouchi¹, Tomoya S. Kitajima^{1,2,*}

Faithful chromosome segregation requires biorientation, where the pair of kinetochores on the chromosome establish bipolar microtubule attachment. The integrity of the kinetochore, a macromolecular complex built on centromeric DNA, is required for biorientation, but components sufficient for biorientation remain unknown. Here, we show that tethering the outer kinetochore heterodimer NDC80-NUF2 to the surface of apolar microbeads establishes their biorientation-like state in mouse cells. NDC80-NUF2 microbeads align at the spindle equator and self-correct alignment errors. The alignment is associated with stable bipolar microtubule attachment and is independent of the outer kinetochore proteins SPC24-SPC25, KNL1, the Mis12 complex, inner kinetochore proteins, and Aurora. Larger microbeads align more rapidly, suggesting a size-dependent biorientation mechanism. This study demonstrates a biohybrid kinetochore design for synthetic biorientation of microscale particles in cells.

Accurate chromosome segregation during cell division is essential for genome stability. Central to this process is chromosome biorientation, wherein microtubules attach to the pair of kinetochores on the chromosome from the opposite spindle poles. Kinetochores—macromolecular assemblies built on centromeric DNA—consist of >100 different proteins in vertebrates (1, 2). Kinetochore and centromere proteins are categorized into at least three groups: (i) outer kinetochore proteins forming connections with spindle microtubules, (ii) inner kinetochore proteins linking outer kinetochore proteins with centromeric DNA, and (iii) inner centromere proteins localizing between the kinetochore pair (fig. S1). Biorientation requires selective stabilization of bipolar kinetochore-microtubule attachment, which is thought to be achieved by coordinated actions of kinetochore and centromere proteins. One model suggests that biorientation is mediated by spatial separation of kinetochore-microtubule attachment sites from the inner centromere, when microtubules pull the kinetochore pair toward opposite poles (3–8). Consistent with this model, phosphorylation by Aurora, an inner centromere kinase required for biorientation, weakens microtubule binding of outer kinetochore proteins such as the Ndc80 complex (9–11). However, inner centromere localization of Aurora kinase is dispensable for accurate chromosome segregation (12–14), suggesting the existence of additional biorientation mechanisms. An alternative model suggests that kinetochores intrinsically stabilize microtubule attachment upon tension (15, 16). Consistent with this model, purified yeast kinetochores containing nearly

the complete set of kinetochore proteins, but lacking Aurora, directly stabilize microtubule attachment upon tension *in vitro* (15). This tension-dependent stabilization relies on the recruitment of Stu2 (known as chTOG in mammals) to the Ndc80 complex (16, 17). However, whether the outer kinetochore Ndc80 branch alone is sufficient for biorientation in cells remains unclear.

Results

NDC80-NUF2 enables microbeads to align

The NDC80-NUF2 heterodimer is an outer kinetochore subcomplex that contains microtubule-binding domains at their N termini (Fig. 1A). It serves as a major anchor for kinetochore-microtubule attachment (10, 11, 18, 19). We hypothesized that NDC80-NUF2 recapitulates the microtubule-binding properties of kinetochores when bound to the surface of microbeads. Mouse oocytes were chosen as a model living system for functional assays because microbeads can be microinjected into them at the prophase-arrested stage, and the oocytes can be released synchronously into M phase (meiosis I). We microinjected mRNAs encoding C-terminally green fluorescent protein-tagged NDC80 (NDC80-GFP) and NUF2, followed by anti-GFP-conjugated microbeads (1.7 to 2.6 μm in diameter), into the cytoplasm, and then induced M phase (Fig. 1A and movie S1). At metaphase, microbeads coated with NDC80-GFP and NUF2 (Fig. 1B; hereafter called NDC80-NUF2 microbeads) were located near chromosomes, whereas control GFP-coated microbeads were located away from chromosomes, presumably outside the spindle (fig. S2A). Furthermore, three-dimensional (3D) inspection revealed that NDC80-NUF2 microbeads were well aligned at the metaphase plate (fig. S2, A and B). This observation suggests that NDC80-NUF2 recruitment enables microbeads to align at the metaphase plate.

Alignment by NDC80-NUF2-specific properties

We investigated whether NDC80-NUF2-specific properties aligned microbeads. First, we tested other outer kinetochore components. KNL1 is an outer kinetochore protein with a microtubule-binding domain at its N terminus (10, 20). Microbeads binding to C-terminally GFP-tagged KNL1 (KNL1-GFP) did not align in the spindle (fig. S2, A and B). The Mis12 complex (DSN1-MIS12-NSL1-PMF1/NNF1) recruits the Ndc80 complex (NDC80-NUF2-SPC24-SPC25) at the outer kinetochore (10). Consistent with this recruitment mechanism, coexpression of NSL1-GFP with MIS12 and DSN1 allowed microbeads to recruit NDC80 (fig. S2C) and align in the spindle (fig. S2, A and B). Next, we tested microtubule-binding proteins. The GFP fusion of neither the microtubule-associated protein MAP4 (21), the microtubule plus-end protein EB3 (21), nor the antiparallel microtubule cross-linker PRC1 efficiently aligned microbeads (fig. S2, A and B). Furthermore, we deleted or mutated the loop domain of NDC80, which is critical for its microtubule binding (22–24). The loop deletion or mutation significantly perturbed microbead alignment (fig. S2D). In oocytes treated with the small-molecule inhibitor monastrol, the loop deletion or mutation positioned microbeads significantly farther from the monopolar spindle (fig. S2E), suggesting that the NDC80 loop promotes microtubule binding on microbeads, as it does on kinetochores (22–24). Quantification of fluorescence signals suggested that the density of NDC80-NUF2 dimer on microbeads was substantially lower than that on kinetochores (fig. S2F), consistent with the idea that anti-GFP-mediated NDC80 tethering was unable to bypass the requirement of the loop-mediated NDC80-NDC80 clustering for efficient microtubule binding (24). Finally, expression of NDC80-GFP alone without NUF2 did not efficiently align microbeads (fig. S2D), suggesting that NDC80-NUF2 heterodimerization, likely facilitated by an exogenous supply of NUF2, is critical. These results suggest that NDC80-NUF2 heterodimer-specific properties enable microbead alignment.

Efficient alignment

3D live imaging of NDC80-NUF2 microbeads showed that they gradually aligned with kinetics similar to chromosomes (Fig. 1, C to F, and movie S2). Kymograph analysis showed that the alignment of NDC80-NUF2 microbeads was stably maintained until anaphase onset, as observed for chromosomes (Fig. 1D). NDC80-NUF2 microbeads occupied the inner region of the metaphase plate, whereas chromosomes were ejected to the outer region (Fig. 1D and fig. S3A). The microbeads were aligned at regular intervals similar to chromosomes (fig. S3B). Thus, NDC80-NUF2 microbeads establish stable alignment with a preference for positioning at the inner region of the

¹Laboratory for Chromosome Segregation, RIKEN Center for Biosystems Dynamics Research (BDR), Kobe, Japan. ²Graduate School of Biostudies, Kyoto University, Kyoto, Japan.

*Corresponding author. Email: tomoya.kitajima@riken.jp

Fig. 1. NDC80-NUF2 suffices for microbead alignment. (A) Experimental design. NDC80-NUF2 beads were constructed through the coexpression of NDC80-GFP and NUF2 by mRNA microinjection, followed by anti-GFP bead microinjection, into the cytoplasmic region near the nucleus of prophase-arrested germlinal vesicle (GV) stage mouse oocytes. Bead dynamics were monitored after the induction of meiotic resumption. (B) NDC80-NUF2 beads. Oocytes expressing NDC80-GFP and NUF2-HA (hemagglutinin) and carrying anti-GFP beads at metaphase [5 hours after nuclear envelope breakdown (NEBD)] were immunostained with anti-HA and Hoechst33342. Structured illumination microscopy was used. Scale bars, 10 μm (top) and 2 μm (bottom).

(C) Live confocal imaging. 3D-reconstructed and z-projection images of chromosomes (H2B-mCherry, magenta) and NDC80-NUF2 beads (green). Time after NEBD (hours:minutes). Scale bar, 10 μm. (D) Kymograph. Images in (C) were kymographed with projected signals on the basis of the spindle axis. The vertical axis of the kymographs shows the distance from the spindle equator (left) and the distance from the spindle axis (right), respectively. (E) Alignment efficiency. The distances of NDC80-NUF2 beads and chromosomes from the spindle equator were quantified. Simulated random distribution of particles within a spindle-like ellipsoid (20 or 30 μm in length at 2 or 6 hours, respectively, and 20 μm in width) is used as a reference. The number of beads or chromosomes (from 14 oocytes in three independent experiments) is indicated in parentheses. P values were calculated with Kruskal-Wallis test with Dunn's correction. (F) Misalignment frequency. Fractions of misaligned NDC80-NUF2 beads and chromosomes in (E) are shown. "Misaligned" refers to positions >5 μm from the spindle equator. Each dot shows the data of an oocyte. P values were calculated with Fisher's exact test.

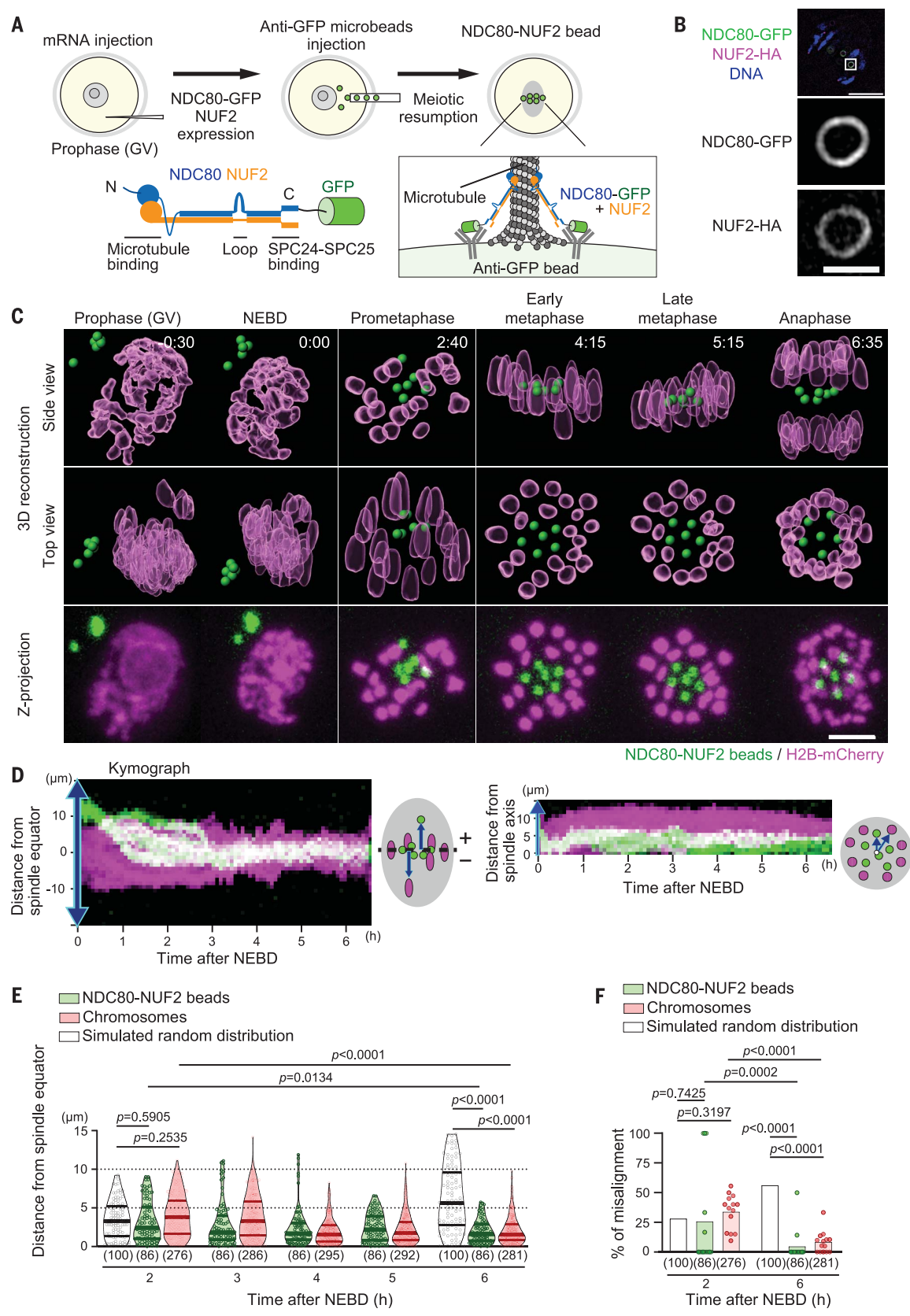
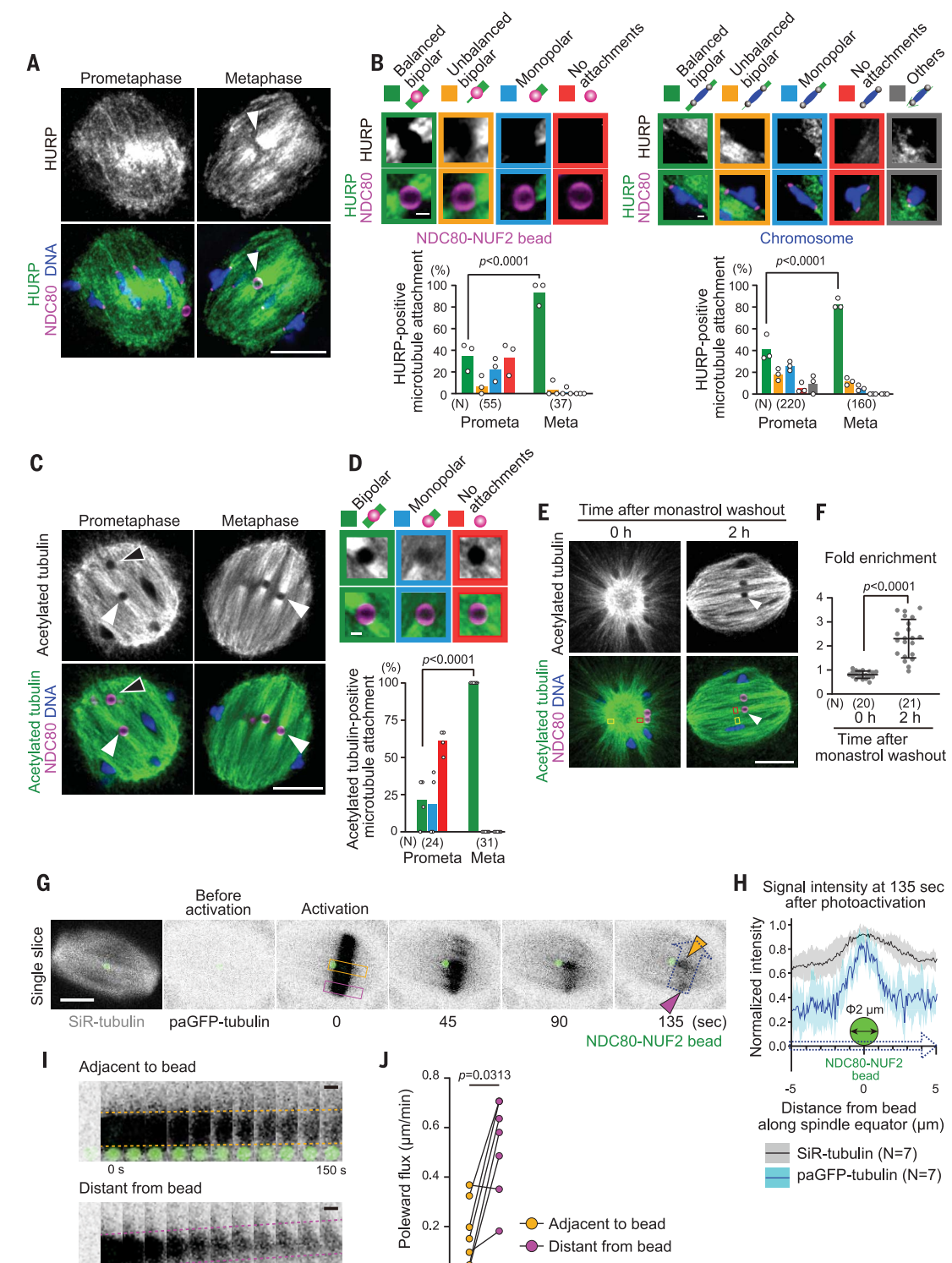


Fig. 2. Bipolar microtubule attachment stabilized without active plus-end assembly.

(A) Bipolar attachment on aligned microbeads. Confocal single-slice images of oocytes carrying NDC80-NUF2 beads, immunostained for NDC80-GFP (kinetochores and NDC80-NUF2 beads, magenta), HURP (green), and DNA (Hoechst33342, blue) at 3 hours (prometaphase) and 5 hours (metaphase) after NEBD. The white arrowhead indicates an NDC80-NUF2 bead with bipolar attachment. Note that the signals of NDC80-GFP uniformly located on the bead surface appear as a pair of crescents owing to an artifact with confocal laser scanning microscopy (fig. S9). Scale bar, 10 μm .

(B) Quantification of attachments. Attachment of HURP bundles with beads and chromosomes are categorized and magnified. Scale bars, 1 μm . The number of chromosomes and beads are indicated in parentheses (from 11 prometaphase and 8 metaphase oocytes, respectively, in three independent experiments). Each dot shows the data of one experiment. P values were calculated with Fisher's exact test.



(C) Stable microtubule attachment. Oocytes were stained with anti-acetylated tubulin, and attachments were categorized as in (A) and (B). White and black arrowheads indicate aligned and misaligned NDC80-NUF2 beads, respectively. Scale bars, 10 μm (C) and 1 μm (D). The number of beads in four prometaphase and five metaphase oocytes is indicated in parentheses. Each dot shows the average of an oocyte. P values were calculated with Fisher's exact test.

(D) Tension-dependent stable attachment. Oocytes were treated with monastrol and then released by washout. Oocytes were immunostained with anti-acetylated tubulin. The white arrowhead indicates an NDC80-NUF2 bead with bipolar attachment. Fold enrichment is the fluorescence intensity in regions adjacent to beads (red rectangle) relative to that in the other regions (yellow rectangle). Scale bar, 10 μm . The number of beads from five (0 hours) and four (2 hours) oocytes are indicated in parentheses. P values were calculated with unpaired Welch's t test.

(E) Fluorescence decay after microtubule photoactivation. Oocytes expressing photoactivatable GFP (paGFP)-tubulin, NDC80-mCherry, and NUF2 and carrying an anti-RFP (red fluorescent protein) bead were cultured in the presence of SiR-tubulin. Photoactivation was performed along the equator of the metaphase spindle. Orange and magenta arrowheads indicate fluorescence signals stably maintained adjacent to the bead and distant from the bead, respectively. Scale bar, 10 μm .

(F) Enrichment of stable microtubules. Images at 135 s after photoactivation were used to generate plot profiles on a line along the photoactivated region [cyan dotted arrow in (G)]. Mean and SD are shown. The number of oocytes from two independent experiments is indicated in parentheses.

(G) Signal intensity at 135 sec after photoactivation

(H) Signal intensity at 135 sec after photoactivation

(I) Signal intensity at 135 sec after photoactivation

(J) Signal intensity at 135 sec after photoactivation

shown as orange and magenta rectangles in (G) were kymographed. Scale bar, 2 μm . (J) Slow poleward flux. The poleward flux of photoactivated tubulin signals was calculated. Note that signals adjacent to the bead (orange) moved slower than those distant from the bead (magenta), indicating less active microtubule plus-end assembly. P values were calculated with Wilcoxon matched-pairs signed-rank test.

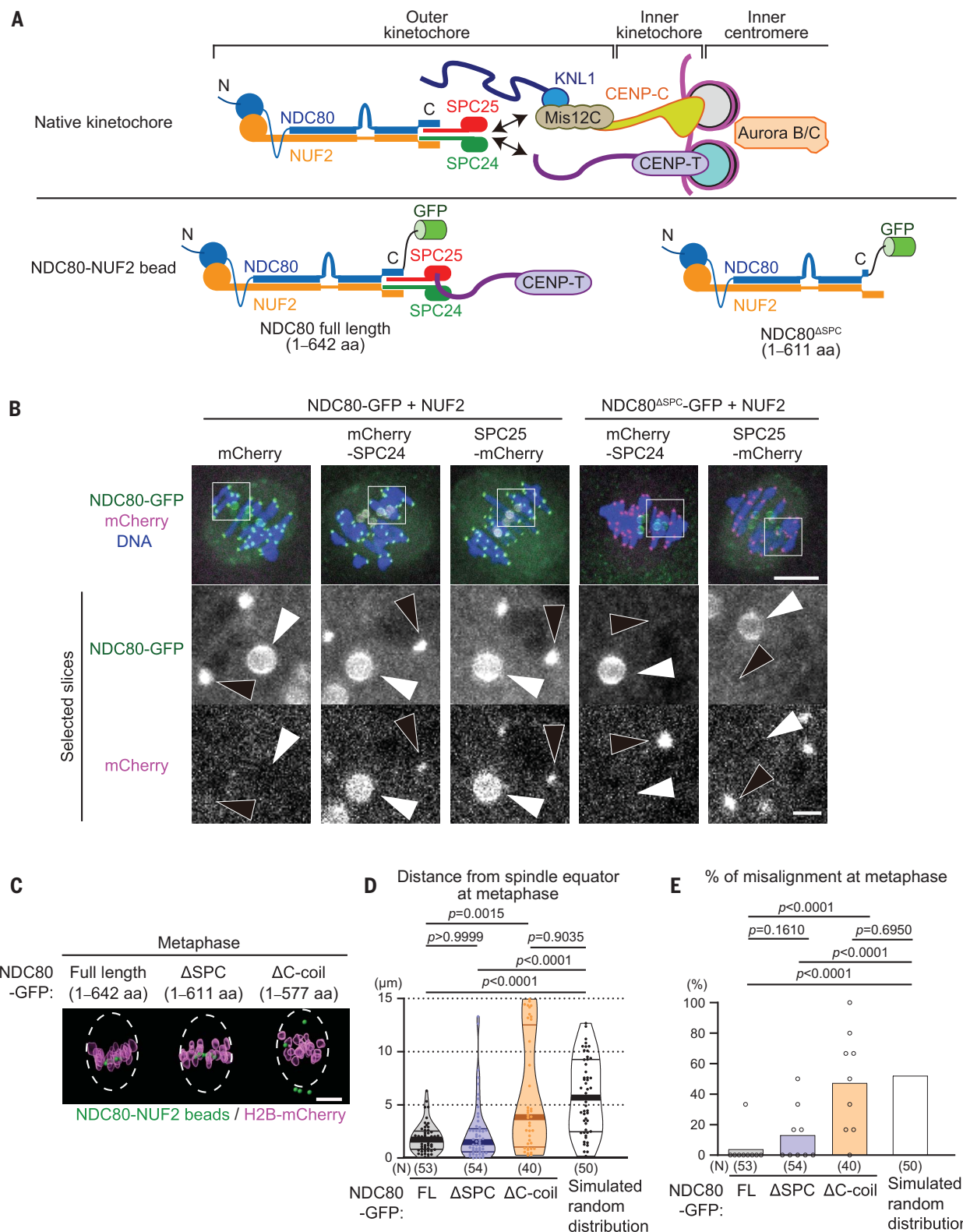


Fig. 3. Alignment independent of SPC24-SPC25, KNL1, the Mis12 complex, the inner kinetochore, and Aurora. (A) Composition of native kinetochores and NDC80-NUF2 beads. In the native kinetochore, NDC80-NUF2 binds to SPC24-SPC25, which binds to the Mis12 complex (Mis12C) and CENP-T.

Mis12C binds to KNL1 and CENP-C. The NDC80-NUF2-SPC24-SPC25 complex, KNL1, and Mis12C forms the outer kinetochore KMN network (10). The inner kinetochore proteins CENP-T and CENP-C link the outer kinetochore to centromeric nucleosomes. Aurora B and its germ cell-specific homolog Aurora C (34) are enriched at the inner centromere. NDC80-NUF2 beads recruit SPC24-SPC25 and CENP-T from the endogenous pool, whereas NDC80^{ASPC}-NUF2 beads do not, as shown in (B) and fig. S5, A and E, aa, amino acids. (B) NDC80-NUF2 beads recruit SPC24-SPC25, but NDC80^{ASPC}-NUF2 beads do not. Indicated proteins were expressed in oocytes carrying anti-GFP beads. Oocytes were fixed 5 hours after NEBD and immunostained for NDC80-GFP (green), mCherry (magenta), and DNA (Hoechst33342, blue). Z-projection images are shown. Black and white arrowheads indicate kinetochores and beads, respectively. Note that the signals of NDC80-GFP uniformly located on the bead surface appear as a pair of crescents owing to an artifact with confocal laser

scanning microscopy (fig. S9). Scale bars, 10 μm (top) and 2 μm (bottom). For quantification, see fig. S5A. (C) NDC80^{ASPC}-NUF2 beads have alignment capability. 3D-reconstructed images of chromosomes (H2B-mCherry, magenta) and beads (NDC80-GFP, green) at 6 hours after NEBD. In contrast to NDC80^{ASPC}-NUF2 beads, NDC80^{AC-coil}-NUF2 beads failed to align. Dashed lines indicate estimated spindle shape (20 μm in width and 30 μm in length). Scale bar, 10 μm . (D) Alignment of NDC80^{ASPC}-NUF2 beads. Distance of beads from the spindle equator was quantified. The number of beads (in each case, from nine oocytes in three independent experiments) is indicated in parentheses. Simulated random distribution of particles within a spindle-like ellipsoid (30 μm in length and 20 μm in width) is used as a reference. *P* values were calculated with Kruskal-Wallis test with Dunn's correction. FL, full length. (E) Misalignment frequency. "Misaligned" refers to positions >5 μm from the spindle equator. Each dot shows the fraction in one oocyte. *P* values were calculated with Fisher's exact test.

metaphase plate during meiosis I in oocytes. Alignment of NDC80-NUF2 microbeads was similarly observed during meiosis II in oocytes and during the first mitosis in embryos (fig. S3C and movies S3 and S4).

Robust alignment

Metaphase is occasionally accompanied by one or a few misaligned chromosomes, which are normally corrected to align by anaphase onset. Similarly, one or two NDC80-NUF2 microbeads were occasionally misaligned in early metaphase (fig. S3D). Tracking these microbeads showed their transient poleward movement, which was subsequently corrected to a movement toward the metaphase plate, resulting in recovery of alignment (fig. S3, D to F, and movie S5). Consequently, at 5 min before anaphase onset, all of the NDC80-NUF2 microbeads were aligned ($n = 84$ in 14 oocytes) within 5 μm from the spindle equator (fig. S3G). Thus, like chromosomes, NDC80-NUF2 microbeads can correct their own misalignment.

Bipolar microtubule attachment

Using the kinetochore fiber marker HURP, we examined whether NDC80-NUF2 microbeads establish bipolar microtubule attachment (25). At metaphase, when microbeads and chromosomes were fully aligned, the vast majority of NDC80-NUF2 microbeads (34/37, 92%) showed bipolar attachment to the end of HURP-decorated microtubule bundles, similar to the kinetochore pair of chromosomes (Fig. 2, A and B, "Metaphase"; movie S6). In contrast, at prometaphase, when alignment was not completed, bipolar attachment was less frequent (Fig. 2, A and B, "Prometaphase"). At this stage, aligned microbeads were more frequently attached to bipolar HURP-decorated microtubule bundles than were unaligned microbeads (fig. S4A), as observed for chromosomes (Fig. 2, A and B, and fig. S4A). Furthermore, acetylated tubulin, a marker for relatively stable microtubules (26), was enriched on microtubule bundles attached to NDC80-NUF2 microbeads at metaphase (Fig. 2, C and D). No such enrichment was observed in the monopolar spindle of monastrol-treated oocytes (Fig. 2, E and F). These results suggest that alignment of NDC80-NUF2 microbeads is associated with bipolar end-on attachment to tension-stabilized microtubule fibers. On the basis of these results and the fact that they stably align, we conclude that NDC80-NUF2 microbeads establish a biorientation-like state.

No detectable cold-stable microtubule fibers

Kinetochore fibers—microtubule bundles with end-on attachment to kinetochores—are characterized by their cold stability. In oocytes, cold-stable kinetochore fibers are rarely observed at early metaphase, when most chromosomes are aligned, and then gradually increase during metaphase (27, 28). Whether the increase in cold-stable kinetochore fibers is required for alignment maintenance is unknown. We found that at metaphase, when alignment was completed, only 7% (2/28) of NDC80-NUF2 microbeads were attached to cold-stable microtubule fibers, whereas 68% (109/160) of chromosomes were (fig. S4, B and C). These results suggest that NDC80-NUF2 microbeads are defective in forming attachment with cold-stable microtubule bundles and that cold-stable attachment is dispensable for maintaining a biorientation-like state.

Stable microtubule attachment without promoting plus-end assembly

To measure microtubule stability more directly, we monitored fluorescence decay after photoactivation of microtubules (Fig. 2G and fig. S4D). Analysis of the decay fitted to a double exponential curve (11, 29) revealed a substantial enrichment of slowly decaying microtubules adjacent to NDC80-NUF2 microbeads at metaphase (Fig. 2H). The half-life of the microbead-adjacent stable microtubules was 3.8 ± 2.2 min, comparable to that of stable microtubules in other spindle regions presumably containing kinetochore microtubules (fig. S4E) (30). These results show that NDC80-NUF2 microbeads attach to microtubules as stably as kinetochores.

Kinetochore-microtubule attachment is fully stabilized by a tension-promoted switch from microtubule plus-end disassembly to assembly (15). To investigate whether NDC80-NUF2 microbeads stabilize attachment through similar mechanisms, we analyzed the poleward flux of photoactivated tubulin (Fig. 2G) as a readout of microtubule plus-end assembly. The poleward flux velocity of microbead-adjacent stable microtubules was 0.17 ± 0.13 $\mu\text{m}/\text{min}$, significantly slower than that of other spindle regions presumably containing kinetochore microtubules (0.52 ± 0.20 $\mu\text{m}/\text{min}$) (Fig. 2, I and J) (31). Thus, NDC80-NUF2 microbeads establish highly stable microtubule attachment without promoting plus-end assembly, unlike kinetochores.

Alignment independent of SPC24-SPC25, KNL1, the Mis12 complex, and inner kinetochore proteins

We speculated that NDC80-NUF2 microbeads acquire a biorientation-like state by recruiting kinetochore and centromere proteins from the endogenous pool. NDC80-NUF2 microbeads recruited SPC24 and SPC25, likely forming the Ndc80 complex (19) (Fig. 3, A and B, and fig. S5A), but no detectable levels of KNL1 or the Mis12 complex components DSNI or PMF1 (fig. S5B). SKA1 and SKA3, components of the Ska complex that interacts with NDC80-NUF2 in somatic cells (23, 32), were enriched on microbeads but not detected on kinetochores in oocytes (fig. S5C). chTOG, which interacts with NDC80-NUF2 in somatic cells (16, 17), was not detected on kinetochores in oocytes (33) or on microbeads (fig. S5D). The inner kinetochore protein CENP-T, but neither CENP-C nor the inner centromere protein Aurora B or C (34), was detected on microbeads (fig. S5, E to G). We conclude that NDC80-NUF2 microbeads establish stable alignment independently of the recruitment of KNL1, the Mis12 complex, CENP-C, and Aurora B and C (Fig. 3A).

SPC24-SPC25 bridges the C-terminal domains of NDC80-NUF2 to the Mis12 complex or CENP-T (Fig. 3A) (1, 2). When we deleted a short segment of the C terminus (amino acids

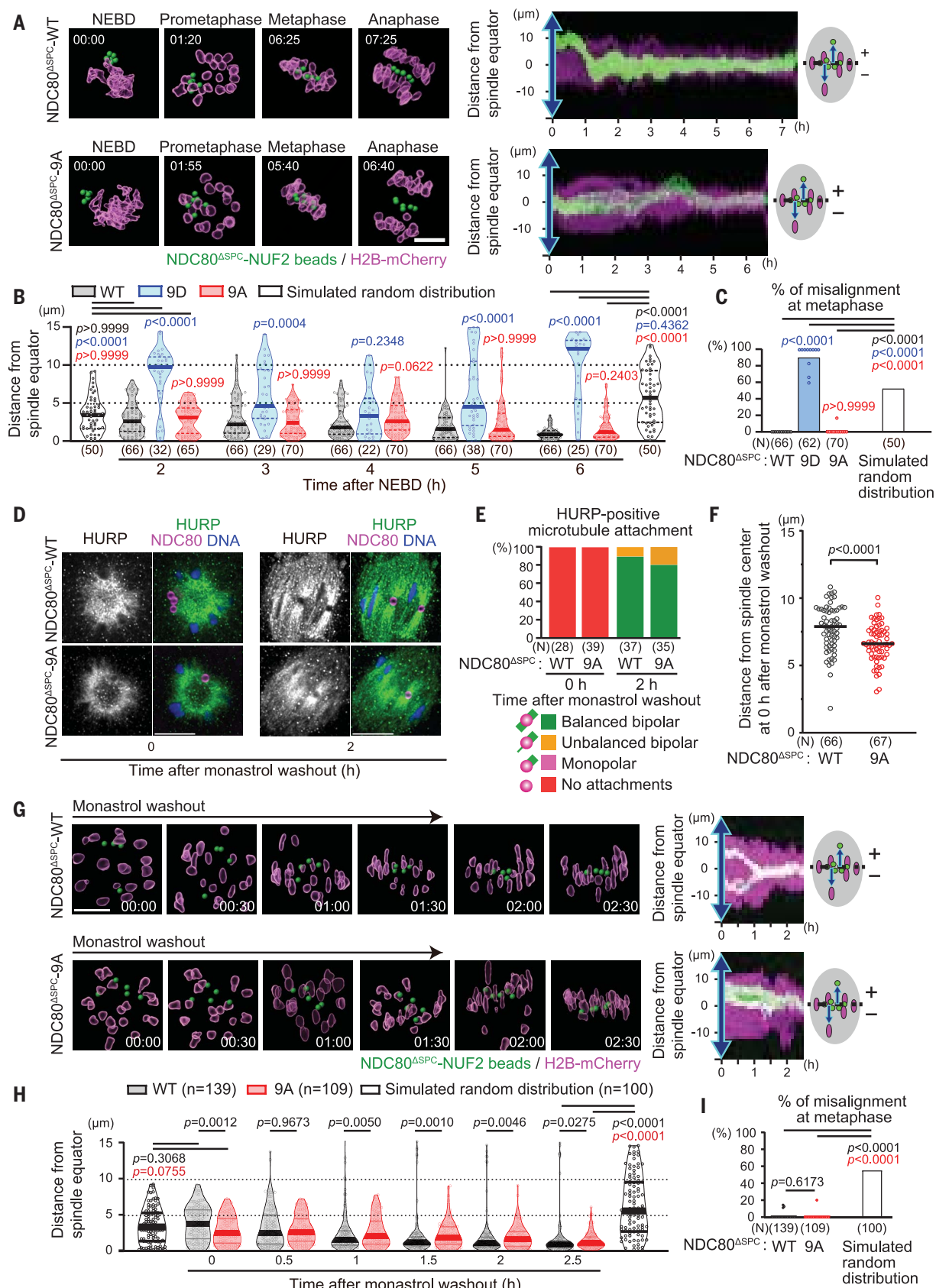


Fig. 4. Alignment independent of NDC80 phosphoregulation. (A) Live imaging. 3D-reconstructed images of chromosomes (H2B-mCherry, magenta) and NDC80^{ΔSPC}-WT/9A-NUF2 beads (green; WT, wild type). Time after NEBD (hours:minutes). Scale bar, 10 μm. The kymograph shows projected signals on the spindle axis

over time. The vertical axis shows distance from the spindle equator. Images for NDC80^{ASPC}-9D-NUF2 acquired in the same experiment are shown in fig. S7A. (B) Alignment efficiency. Distance of NDC80^{ASPC}-WT/9A/9D-NUF2 beads from the spindle equator was quantified. The number of beads (from 11, 11, and 12 oocytes, respectively, in three independent experiments) is indicated in parentheses. Simulated random distribution of particles within a spindle-like ellipsoid (20 or 30 μm in length at 2 or 6 hours, respectively, and 20 μm in width) is used as a reference. NDC80^{ASPC}-9D-NUF2 beads apparently positioned outside the spindle ($>10 \mu\text{m}$ from the spindle axis or $>15 \mu\text{m}$ from the equator) were excluded from the analysis. P values against WT or simulated values were calculated using Kruskal-Wallis test with Dunn's correction. (C) Misalignment frequency. "Misaligned" refers to positions $>5 \mu\text{m}$ from the spindle equator at 6 hours after NEBD. Each dot shows the data of an oocyte. P values were calculated with Fisher's exact test. (D) Microtubule attachment. Confocal single-slice images of oocytes after monastrol washout, immunostained for GFP (NDC80^{ASPC}-GFP, white), HURP (green), and DNA (Hoechst33342, blue). Scale bars, 10 μm . (E) Attachments with microtubule bundles in (D) are categorized and quantified.

612 to 642) of NDC80 (the resulting form is hereafter called NDC80^{ASPC}) (Fig. 3A), NDC80^{ASPC}-NUF2 microbeads contained no detectable SPC24-SPC25 or CENP-T (Fig. 3B and fig. S5, A and E). Consistent with these observations, NDC80^{ASPC}-GFP did not localize to kinetochores (Fig. 3B and fig. S6A). Nevertheless, NDC80^{ASPC}-NUF2 microbeads established alignment, similar to NDC80-NUF2 microbeads (Fig. 3, C to E), whereas NDC80^{AC-coil}-NUF2, in which a larger segment of the C terminus (amino acids 578 to 642) of NDC80 was deleted, failed to align microbeads (Fig. 3, C to E). These results suggest that NDC80-NUF2 microbeads establish a biorientation-like state independently of the recruitment of SPC24-SPC25 and its inner kinetochore interactors such as CENP-T.

The alignment defect of NDC80^{AC-coil}-NUF2 microbeads led us to address whether PRC1, which interacts with the C-terminal region of NDC80 in mouse oocytes and was enriched on NDC80-NUF2 microbeads (fig. S5B) (35), mediates microbead alignment. NDC80^{AC-coil}-NUF2 microbeads showed significantly reduced but still substantial PRC1 enrichment (fig. S6B). Additional tethering or overexpression of PRC1 did not rescue NDC80^{AC-coil}-NUF2 microbead alignment (fig. S6C). Thus, the alignment ability of microbeads does not simply correlate with their PRC1 levels, although the possibility that PRC1 is involved in microbead alignment is not excluded.

Alignment independent of NDC80 phosphoregulation

Chromosome biorientation depends on Aurora-mediated phosphorylation of the N-terminal tail of NDC80, which weakens microtubule-binding of NDC80-NUF2 for attachment error correction (3, 4, 8, 10, 11). Consistent with the idea that NDC80-NUF2 microbeads align through their microtubule-binding activity, NDC80^{ASPC}-9D-NUF2 microbeads, which carry phosphomimetic mutations, failed to align (fig. S7A). In contrast, phosphodeficient NDC80^{ASPC}-9A-

NUF2 microbeads aligned with comparable kinetics to NDC80^{ASPC}-NUF2 microbeads (Fig. 4, A to C, and movie S7). Consistent with this observation, NDC80-NUF2 microbeads aligned in oocytes treated with AZD1152, an inhibitor of both Aurora B and C (28), whereas chromosomes misaligned (fig. S7, B to D). Thus, Aurora-mediated phosphorylation of the NDC80 tail is dispensable for NDC80-NUF2 microbead alignment.

NDC80 phosphoregulation promotes alignment under a challenging condition

One of the most stringent tests for the capacity of biorientation is a monastrol washout assay (36). In monastrol-treated oocytes, NDC80^{ASPC}-NUF2 microbeads were located around the surface of the monopolar spindle, similar to chromosomes, with no attachment to HURP-positive microtubule bundles (Fig. 4, D and E, "0 h"). Notably, NDC80^{ASPC}-9A-NUF2 microbeads were significantly more inwardly located (Fig. 4F), although attachment to HURP-positive microtubule bundles was not observed (Fig. 4, D and E, "0 h"). These results suggest that NDC80-NUF2 microbeads suppress monopolar attachment of HURP-negative microtubules by means of NDC80 tail phosphorylation.

Upon monastrol washout, NDC80^{ASPC}-NUF2 microbeads gradually aligned, in a manner similar to chromosomes (Fig. 4, G and I, and movie S8). The aligned microbeads were attached with bipolar HURP-positive microtubule bundles (Fig. 4, D and E, "2 h"). Similar observations were made with acetylated tubulin (Fig. 2, E and F). NDC80^{ASPC}-9A-NUF2 microbeads also established alignment after monastrol washout (Fig. 4, G to I), with bipolar attachment of HURP-positive microtubule bundles (Fig. 4, D and E). Thus, NDC80 tail phosphorylation is dispensable for a biorientation-like state. However, the alignment of NDC80^{ASPC}-9A-NUF2 microbeads was significantly delayed compared with NDC80^{ASPC}-NUF2 microbeads (Fig. 4H). Thus, the phosphoregulation of the NDC80

The number of beads (from 7, 9, 9, and 9 oocytes, respectively, in three independent experiments) is shown in parentheses. (F) NDC80^{ASPC}-9A-NUF2 beads are located inwardly. In monastrol-treated oocytes, the positions of NDC80^{ASPC}-WT/9A-NUF2 beads were analyzed. The number of beads (from 26 and 20 oocytes, respectively, in three independent experiments) is shown in parentheses. P value was calculated using unpaired Welch's t test. (G) Live imaging. 3D-reconstructed images of chromosomes (H2B-mCherry, magenta) and NDC80^{ASPC}-WT/9A-NUF2 beads (green) after monastrol washout. Time after monastrol washout (hours:minutes). Scale bar, 10 μm . Kymographs along the spindle axis are shown. (H) Alignment efficiency. Distance of NDC80^{ASPC}-WT/9A-NUF2 beads from the spindle equator after monastrol washout was quantified as in (B). The number of beads (from 28 and 22 oocytes, respectively, in three independent experiments) is indicated in parentheses. P values were calculated using Mann-Whitney U test. (I) Misalignment frequency. "Misaligned" refers to positions $>5 \mu\text{m}$ from the spindle equator at 2.5 hours after monastrol washout. Each dot shows the data of an oocyte. P values were calculated with Fisher's exact test.

tail is required for NDC80-NUF2 microbeads to efficiently establish a biorientation-like state for recovery from challenging conditions.

Large bead size promotes alignment

NDC80-NUF2 microbeads were 1.7 to 2.6 μm in diameter, an order of magnitude larger than kinetochores ($\sim 250 \text{ nm}$ wide) (37, 38). To test size-dependent effects, we co-injected smaller microbeads ranging from 0.4 to 1.7 μm in diameter, together with larger microbeads (1.7 to 2.6 μm), into the same oocytes (Fig. 5A). Smaller NDC80-NUF2 microbeads aligned significantly less efficiently (Fig. 5, B to D). This was unlikely to be due to a difference in NDC80-NUF2 density, as the smaller and larger microbeads did not differ significantly in mean NDC80 fluorescence intensity (fig. S8A). Moreover, the alignment delay of smaller microbeads was not significantly prolonged by AZD1152 treatment (fig. S8, B and C). These results suggest that the large size of NDC80-NUF2 microbeads facilitates their alignment independently of bypassing the requirement of Aurora kinase for biorientation.

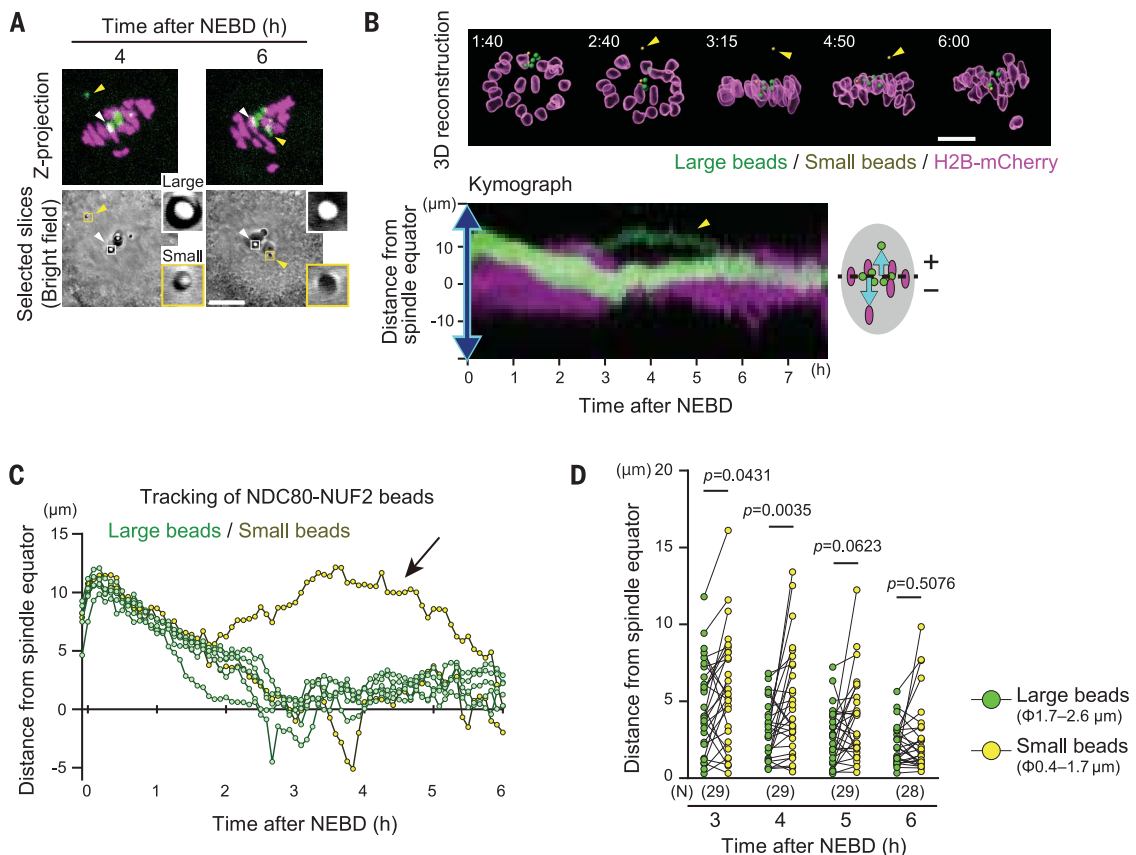
Discussion

We have demonstrated that microbeads tethering NDC80-NUF2 establish a biorientation-like state within the spindle. Previous studies have shown that tethering the fungal outer kinetochore Dam1/DASH complex to sister DNAs allows biorientation depending on other kinetochore proteins and Aurora (39, 40). Studies using vertebrate cells induced ectopic kinetochore assembly with inner kinetochore proteins such as CENP-T or CENP-C tethered to sister DNAs, which fully supported chromosome segregation (41, 42). A recent study shows that genetically encoded nanoscale particles tethering CENP-T recruit kinetochore proteins interacting with microtubules (43). Our study used a biohybrid approach with a microscale bead tethering NDC80-NUF2 to its surface, showing the emergence of the capacity to establish

Fig. 5. Large platform size promotes NDC80-NUF2 microbead alignment.

(A) NDC80-NUF2 beads of different sizes. NDC80-GFP and NUF2 were expressed in oocytes carrying anti-GFP beads of different sizes. Z-projection and selected slice images of NDC80-GFP (green) and H2B-mCherry (magenta) are shown. White and yellow arrowheads indicate beads of 1.9 μm ("Large") and 1.1 μm ("Small") in diameter, respectively, which are magnified in insets. Scale bar, 10 μm. (B) Smaller NDC80-NUF2 microbeads exhibit less efficient alignment. 3D-reconstructed images of chromosomes (H2B-mCherry, magenta) and NDC80-NUF2 beads of different sizes (large beads, green; small beads, yellow, indicated by arrowheads). Time after NEBD (hours: minutes). Scale bar, 10 μm. Kymographs were generated with projected signals on

the basis of the spindle axis. The vertical axis shows the distance from the spindle equator. Arrows indicate a small bead (1.1 μm in diameter). (C) Tracking. Images in (B) were used for tracking. (D) Alignment efficiency. The distances of NDC80-NUF2 beads from the spindle equator were measured. Each dot indicates the average value of beads within one oocyte. Lines connect the data from the same oocytes. The number of oocytes from three independent experiments is indicated in parentheses. *P* values were calculated with Wilcoxon matched-pairs signed-rank test.



a biorientation-like state by bypassing the requirement for the outer kinetochore proteins SPC24-SPC25, KNL1, and the Mis12 complex, the inner kinetochore proteins CENP-T and CENP-C, the inner centromere kinase Aurora, and DNA.

These results suggest that the NDC80-NUF2 branch of the outer kinetochore has an intrinsic mechanism that is sufficient to establish a biorientation-like state when transplanted to microscale particles. NDC80-NUF2 microbeads establish stable bipolar microtubule attachment in a tension-dependent manner. In contrast to kinetochores, where a switch from microtubule plus-end disassembly to assembly allows full attachment stability (15), NDC80-NUF2 microbeads achieve it without promoting plus-end assembly (Fig. 2, G to J). On kinetochores attached to disassembling plus ends, tension can increase attachment stability by suppressing chTOG/Stu2 activity, although not to full stability (16, 17). As chTOG is not enriched on NDC80-NUF2 microbeads (fig. S5D), interaction of NDC80-NUF2 with other proteins, perhaps through the NDC80 loop or C-terminal coiled-coil region, may allow tension-dependent attachment stabilization of micro-

beads. An alternative and not mutually exclusive possibility is that tension promotes attachment stabilization of NDC80-NUF2 microbeads independently of microtubule plus-end dynamics, as previously observed on kinetochores in PtK cells microinjected with the 9G3 antibody (11). In either scenario, the dispensability of microtubule plus-end assembly for NDC80-NUF2 microbeads to achieve full attachment stability is likely due to their unnaturally large size. Consistent with this idea smaller NDC80-NUF2 microbeads align less efficiently (Fig. 5). Our results also suggest that NDC80 phosphorylation, likely by cytoplasmic Aurora, promotes biorientation after monastrol washout. The NDC80-NUF2 branch may intrinsically regulate Aurora activity or its effect in a tension-dependent manner (44).

Our observations shed light on physical requirements for biorientation. First, microbeads without a bipolar cue establish a biorientation-like state, indicating that two physically separate platforms and their geometry, like the sister kinetochores of the mitotic chromosome, are not a prerequisite for establishing bipolar microtubule attachment. This is consistent with

merotelic attachments, where one kinetochore is attached by microtubules from opposite spindle poles, often leading to aneuploidy, particularly in cancer cells (45). Second, alignment efficiency depends on microbead size (Fig. 5), implying that the NDC80-NUF2-mediated biorientation benefits from an expanded platform. Such platform expansion may be attributed to the evolution of the inner kinetochore, which displays self-oligomerization activity (46, 47), and the centromere, which contains DNA arrays that extend to 0.3 to 4.8 mega-base pairs in humans (48). Size-dependent biorientation provides a possible explanation for why microscale NDC80-NUF2 beads align, whereas nanoscale CENP-T particles do not (43). Consistent with these ideas, in Indian muntjac cells, centromere and kinetochore size correlates with both biorientation efficiency and merotelic attachment frequency (49).

Although NDC80-NUF2 microbeads biorient similarly to chromosomes, they differ in their capacity to form cold-stable microtubule attachment with active plus-end assembly. NDC80-NUF2 recruits the Ska complex, which is necessary for kinetochores to establish cold-stable attachment (50) but is not sufficient for

microbeads (figs. S4, B and C, and S5C). Additional tethering of kinetochore or centromere proteins or implementation of spatial regulation of NDC80 phosphorylation (3, 4, 8) may allow NDC80-NUF2 microbeads to establish cold-stable attachment with active plus-end assembly. Moreover, NDC80-NUF2 microbeads are preferentially located in the inner region of the metaphase plate (Fig. 1, C and D, and fig. S3A), perhaps owing to the lack of chromokinesin-mediated polar ejection force (51). Future studies aimed at artificially constructing kinetochores and chromosomes will provide a further understanding of the respective roles of kinetochore, centromere, and chromosome proteins to biorientation. NDC80-NUF2 microbeads align at meiosis I and II and mitosis (fig. S3C and movies S3 and S4), offering their use in various research models such as frog egg extracts and cultured cells where biochemical and mechanical assays are applicable. Kinetochore-like microbeads, together with chromosome-like microbeads inducing spindle self-assembly (52), hold promise as tools for advancing the development of synthetic DNA segregation.

Our artificial kinetochore approach has identified a minimal kinetochore branch that enables an apolar microscale particle to achieve biorientation in live cells. This finding may serve as a foundation for the development of microscale machines or artificial organelles designed to autonomously segregate materials in living systems.

REFERENCES AND NOTES

- I. M. Cheeseman, *Cold Spring Harb. Perspect. Biol.* **6**, a015826 (2014).
- A. Musacchio, A. Desai, *Biology* **6**, 5 (2017).
- T. U. Tanaka et al., *Cell* **108**, 317–329 (2002).
- D. Liu, G. Vader, M. J. M. Vromans, M. A. Lampson, S. M. A. Lens, *Science* **323**, 1350–1353 (2009).
- K. S. K. Uchida et al., *J. Cell Biol.* **184**, 383–390 (2009).
- T. J. Maresca, E. D. Salmon, *J. Cell Biol.* **184**, 373–381 (2009).
- X. Wan et al., *Cell* **137**, 672–684 (2009).
- J. P. I. Welburn et al., *Mol. Cell* **38**, 383–392 (2010).
- S. Biggins et al., *Genes Dev.* **13**, 532–544 (1999).
- I. M. Cheeseman, J. S. Chappie, E. M. Wilson-Kubalek, A. Desai, *Cell* **127**, 983–997 (2006).
- J. G. DeLuca et al., *Cell* **127**, 969–982 (2006).
- Z. Yue et al., *J. Cell Biol.* **183**, 279–296 (2008).
- C. S. Campbell, A. Desai, *Nature* **497**, 118–121 (2013).
- R. C. C. Hengeveld, M. J. M. Vromans, M. Vleugel, M. A. Hadders, S. M. A. Lens, *Nat. Commun.* **8**, 15542 (2017).
- B. Akiyoshi et al., *Nature* **468**, 576–579 (2010).
- M. P. Miller, C. L. Asbury, S. Biggins, *Cell* **165**, 1428–1439 (2016).
- J. A. Herman, M. P. Miller, S. Biggins, *eLife* **9**, e61773 (2020).
- R. R. Wei, J. Al-Bassam, S. C. Harrison, *Nat. Struct. Mol. Biol.* **14**, 54–59 (2007).
- C. Ciferri et al., *Cell* **133**, 427–439 (2008).
- J. Espeut, D. K. Cheerambathur, L. Krenning, K. Oegema, A. Desai, *J. Cell Biol.* **196**, 469–482 (2012).
- M. Schuh, J. Ellenberg, *Cell* **130**, 484–498 (2007).
- D. Varma et al., *Nat. Cell Biol.* **14**, 593–603 (2012).
- G. Zhang et al., *J. Cell Sci.* **125**, 3243–3253 (2012).
- S. Polley et al., *EMBO J.* **42**, e12504 (2023).
- H. H. W. Silljé, S. Nagel, R. Körner, E. A. Nigg, *Curr. Biol.* **16**, 731–742 (2006).
- T. Akera, *Semin. Cell Dev. Biol.* **137**, 38–45 (2023).
- S. Brunet et al., *J. Cell Biol.* **146**, 1–12 (1999).
- S. Yoshida, M. Kaido, T. S. Kitajima, *Dev. Cell* **33**, 589–602 (2015).
- Y. Zhai, P. J. Kronebusch, G. G. Borisy, *J. Cell Biol.* **131**, 721–734 (1995).
- Q.-H. Zhang et al., *J. Cell Biol.* **216**, 3133–3143 (2017).
- G. Fitzhariss, *Development* **136**, 2111–2119 (2009).
- P. J. Huis In 't Veld, V. A. Volkov, I. D. Stender, A. Musacchio, M. Dogterom, *eLife* **8**, e49539 (2019).
- C. So et al., *Science* **364**, eaat9557 (2019).
- A. Z. Balboula, K. Schindler, *PLOS Genet.* **10**, e1004194 (2014).
- S. Yoshida et al., *Nat. Commun.* **11**, 2652 (2020).
- M. A. Lampson, K. Renduchitala, A. Khodjakov, T. M. Kapoor, *Nat. Cell Biol.* **6**, 232–237 (2004).
- C. L. Rieder, *Int. Rev. Cytol.* **79**, 1–58 (1982).
- V. Magidson et al., *Nat. Cell Biol.* **17**, 1134–1144 (2015).
- S. Lacefield, D. T. C. Lau, A. W. Murray, *Nat. Cell Biol.* **11**, 1116–1120 (2009).
- E. Kiermaier, S. Woehler, Y. Peng, K. Mechtl, S. Westermann, *Nat. Cell Biol.* **11**, 1109–1115 (2009).
- K. E. Gascoigne et al., *Cell* **145**, 410–422 (2011).
- T. Hori, W.-H. Shang, K. Takeuchi, T. Fukagawa, *J. Cell Biol.* **200**, 45–60 (2013).
- G. B. Sissoko, E. V. Tarasovets, O. Marescal, E. L. Grishchuk, I. M. Cheeseman, *Nat. Cell Biol.* **26**, 45–56 (2024).
- A. K. de Regt, C. J. Clark, C. L. Asbury, S. Biggins, *Nat. Commun.* **13**, 2152 (2022).
- D. Cimini et al., *J. Cell Biol.* **153**, 517–527 (2001).
- M. Hara et al., *Mol. Cell* **83**, 2188–2205.e13 (2023).
- K. Zhou et al., *Nat. Struct. Mol. Biol.* **29**, 403–413 (2022).
- N. Altelmose et al., *Science* **376**, eabl4178 (2022).
- D. Drpic et al., *Curr. Biol.* **28**, 1344–1356.e5 (2018).
- T. N. Gaitanos et al., *EMBO J.* **28**, 1442–1452 (2009).
- V. Magidson et al., *Cell* **146**, 555–567 (2011).
- R. Heald et al., *Nature* **382**, 420–425 (1996).

ACKNOWLEDGMENTS

We thank S. Yoshida and H. Kyogoku for technical assistance for microbead injection; H. Shibuya and Y. Watabane for providing antibodies; T. Shibata, H. Tanimoto, and H. Hayashi for discussion; J. Ellenberg for a microscope automation macro; the imaging and animal facilities of RIKEN BDR for technical support; and all lab members for discussions and comments. K.A. and Y.Z. are supported by the RIKEN Junior Research Associate program.

Funding: RIKEN intramural grants; RIKEN Pioneering Project “Long-timescale Molecular Chronobiology” (T.S.K.); JSPS KAKENHI 23H04948, 21H02407, and 18H05549 (T.S.K.); Mitsubishi Foundation (T.S.K.).

Author contributions: Conceptualization: K.A. and T.S.K. Methodology: K.A., Y.Z., and O.T. Investigation: K.A., Y.Z., and O.T. Visualization: K.A. and Y.Z. Funding acquisition: T.S.K. Project administration: T.S.K. Supervision: T.S.K. Writing – original draft: K.A., Y.Z., O.T., and T.S.K. Writing – review & editing: K.A., Y.Z., O.T., and T.S.K.

Competing interests: The authors declare that they have no competing financial interests. **Data and materials availability:** Plasmids are available from T.S.K. under a material transfer agreement with RIKEN. All data are available in the main text or the supplementary materials. **License information:** Copyright © 2024 the authors, some rights reserved; exclusive licensee American Association for the Advancement of Science. No claim to original US government works. <https://www.science.org/about/science-licenses-journal-article-reuse>

SUPPLEMENTARY MATERIALS

science.org/doi/10.1126/science.adn5428

Materials and Methods

Figs. S1 to S10

References (53–55)

MDAR Reproducibility Checklist

Movies S1 to S8

Submitted 14 December 2023; resubmitted 24 June 2024

Accepted 16 August 2024

10.1126/science.adn5428